nature communications

Article

https://doi.org/10.1038/s41467-024-53794-1

Infectious parvovirus B19 circulates in the blood coated with active host protease inhibitors

Received: 2 July 2024

Accepted: 20 October 2024

Published online: 05 November 2024

Check for updates

Hyunwook Lee[1,7], Ruben Assaraf[2,3,7], Suriyasri Subramanian[4], Dan Goetschius[4], Jan Bieri[2], Nadia M. DiNunno[4], Remo Leisi[2], Carol M. Bator[1], Susan L. Hafenstein[1,5,6] ✉ & Carlos Ros[2] ✉

The lack of a permissive cell culture system has limited high-resolution structures of parvovirus B19 (B19V) to virus-like particles (VLPs). In this study, we present the atomic resolution structure (2.2 Å) of authentic B19V purified from a patient blood sample. There are significant differences compared to non-infectious VLPs. Most strikingly, two host protease inhibitors (PIs), inter-alpha-trypsin inhibitor heavy chain 4 (ITIH4) and serpinA3, were identified in complex with the capsids in all patient samples tested. The ITIH4 binds specifically to the icosahedral fivefold axis and serpinA3 occupies the twofold axis. The protein-coated virions remain infectious, and the capsid-associated PIs retain activity; however, upon virion interaction with target cells, the PIs dissociate from the capsid prior to viral entry. Our finding of an infectious virion shielded by bound host serum proteins suggests an evolutionarily favored phenomenon to evade immune surveillance and escape host protease activity.

Parvovirus B19 (B19V) is a highly prevalent human pathogen that typically causes a mild childhood rash known as erythema infectiosum or fifth disease. In adults, infection has been frequently associated with more severe diseases, including arthropathy and transient aplastic crisis[1–3]. In pregnant women, B19V can spread transplacentally, leading to fetal complications such as non-immune hydrops fetalis, miscarriage, or fetal demise[4,5]. The frequent detection of B19V in blood donations represents a risk of transmission through the administration of plasma-derived therapeutic products[6]. B19V has a selective tropism for human erythroid progenitor cells in the bone marrow. Essential receptors and intracellular factors required for productive infection are restricted to EPO-dependent erythroid differentiation stages[7,8]. These complex conditions cannot be fully reproduced in cell culture, which presents a significant challenge to the production of sufficient amounts of B19V virions for research purposes[9]. As a result, B19V research has faced significant hurdles, and many aspects of the infection, including its native structure, have remained elusive.

B19V is a small, non-enveloped, single-stranded DNA virus. The 26-nm diameter icosahedral capsid shell is composed predominantly of VP2 (95%) with three copies of the minor structural protein, VP1, per capsid[10]. VP1 differs from VP2 by 227 additional residues in the N-terminus, the so-called VP1 unique region (VP1u), which is proposed to exit through the fivefold channel[11]. Upon interaction with susceptible cells, the capsid undergoes a conformational change that exposes the VP1u domains containing the receptor-binding domain (RBD)[12] and a phospholipase A_2 motif[13]. These steps are essential to allow the RBD to interact with its cognate receptor for virus entry and infection of target erythroid progenitor cells[13].

Antigenic sites have been mapped on the capsid surface for VP2 residues[14–18] as well as VP1u[19]. The VP2 region of the capsid most recognized by antibodies encircles the base of the threefold spike. However, much of what has been learned was driven by the use of virus-like particles (VLPs) and there are significant differences in the immune response against recombinant VP2 capsids compared to VP2/

[1]The Hormel Institute, University of Minnesota, Austin, MN, USA. [2]Department of Chemistry, Biochemistry and Pharmaceutical Sciences, University of Bern, Bern, Switzerland. [3]Graduate School for Cellular and Biomedical Sciences, Bern, Switzerland. [4]The Pennsylvania State College of Medicine, Hershey, PA, USA. [5]Department of Biochemistry, Biophysics and Molecular Biology, University of Minnesota, Minneapolis, MN, USA. [6]Department of Infectious Diseases, Mayo Clinic, Rochester, MN, USA. [7]These authors contributed equally: Hyunwook Lee, Ruben Assaraf. ✉e-mail: hafen@umn.edu; carlos.ros@unibe.ch

VP1 particles or authentic virions[14,20]. The reliance on B19V VLPs has been due to the lack of a cell culture system to generate sufficient B19V infectious particles for high resolution structures. Two previous virus structures reported at 8 and 3.5 Å resolution were solved from VLPs that self-assembled in the absence of VP1[11,21]. Previously, B19V particles were isolated from human serum to generate a moderate-resolution cryoEM map of the native virion (7.5 Å)[22]. However, the resolution of the map limited the interpretation of molecular details. Notably, in this previous work, the virus was purified using cesium chloride (CsCl) and EDTA, which have been shown to cause substantial conformational changes and lead to the generation of empty particles[23,24].

Here, we show the 2.2 Å resolution structure of authentic, infectious B19V obtained from a de-identified patient blood sample using cryogenic-sample electron microscopy (cryoEM)[25] single particle analysis. Besides notable structural differences with non-infectious VLPs, our map revealed that the virion associates with two distinct, specifically bound human host proteins, one binding to the icosahedral fivefold vertex and the other binding across the icosahedral twofold axes. Using cryoEM combined with mass spectrometry, the proteins were identified as serpinA3 and inter-alpha-trypsin inhibitor heavy chain 4 (ITIH4), two human protease inhibitors (PIs) that are upregulated in response to inflammation. Both serpin A3 and ITIH4 interacted with the capsid surface in an orientation that maintained the activity of the proteins in the bound state. The binding of the PIs widely covered the capsid surface and overlapped with known antigenic recognition sites. However, the bound proteins do not inhibit attachment or virus entry as the PIs dissociate upon interaction with host cells prior to virus internalization. B19V in complex with these host PIs was consistently detected in all patient samples tested and across virus genotypes, suggesting an evolutionary advantage. Our results suggest a model of a cloaking mechanism for extracellular trafficking, in which B19V binds acute-phase proteins as a defense against the host.

Results

CryoEM structure of the native B19V capsid

B19V from an infected patient plasma donation was concentrated and purified (see Methods). Fractions containing virions were detected by PCR, pooled, and visualized by negative-staining transmission electron microscopy (TEM) to verify the purity and integrity of the virions. Small, 3 μl aliquots were applied to cryoEM grids, blotted, and vitrified for data collection on the Penn State Titan Krios (https://www.huck.psu.edu/core-facilities/cryo-electron-microscopy-facility). The cryoEM micrographs showed homogeneous virus particles that had uniformly dense interiors and small, globular densities extending from the capsid surface (Fig. 1a).

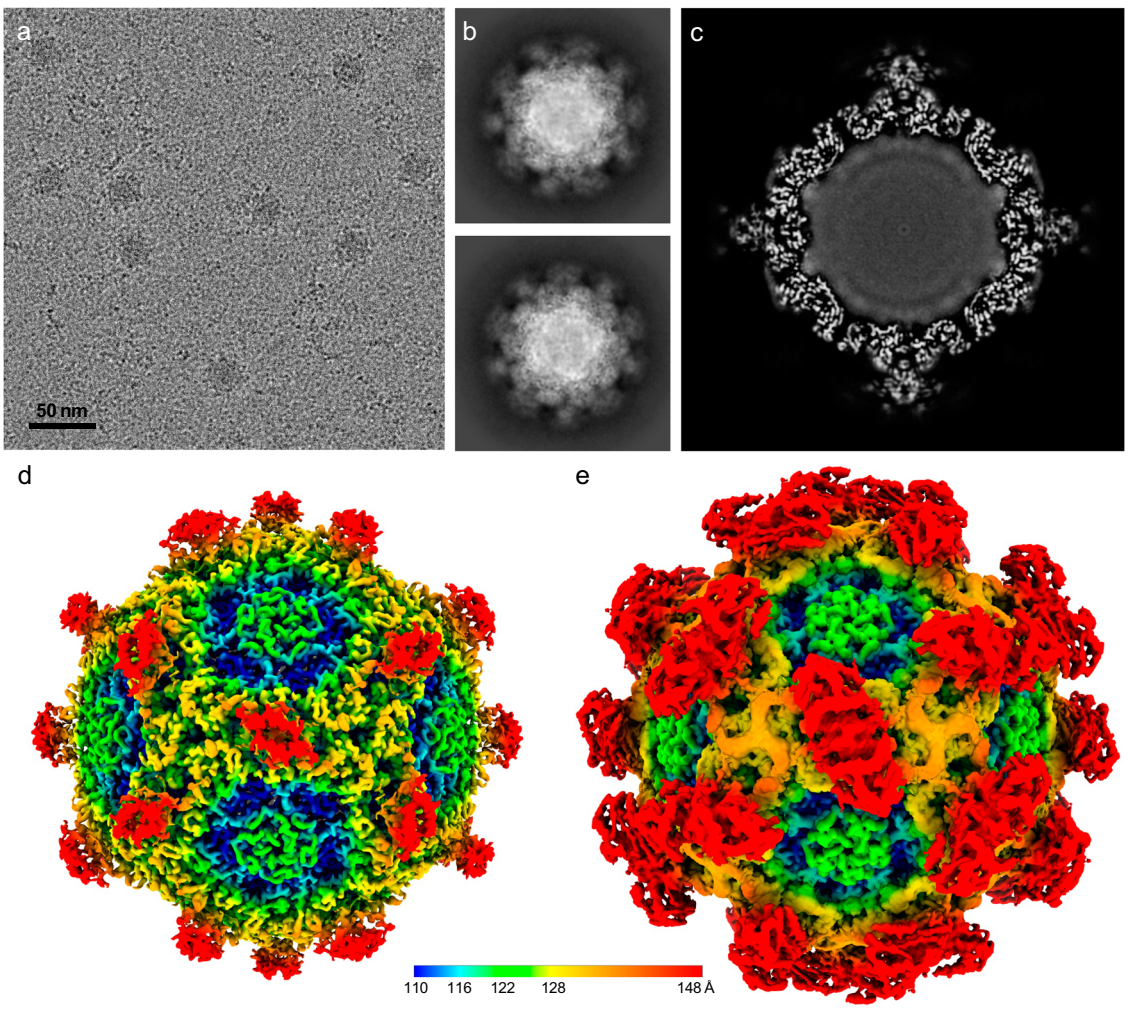

Fig. 1 | CryoEM single particle reconstruction of patient-derived B19V resolved extra density on the icosahedral twofold of the capsid surface. a A representative cryoEM micrograph of the B19V purified from patient serum. (Supplementary Table 1) **b** Representative 2D class average images of the B19V revealing genome-filled capsid with additional densities bound to the capsid surface. **c** Central slab from the icosahedral 3D reconstruction. Surface representations of the icosahedrally averaged map with high (**d**) and low (**e**) contours. The surface is color-coded radially as per the key.

https://doi.org/10.1038/s41467-024-53794-1

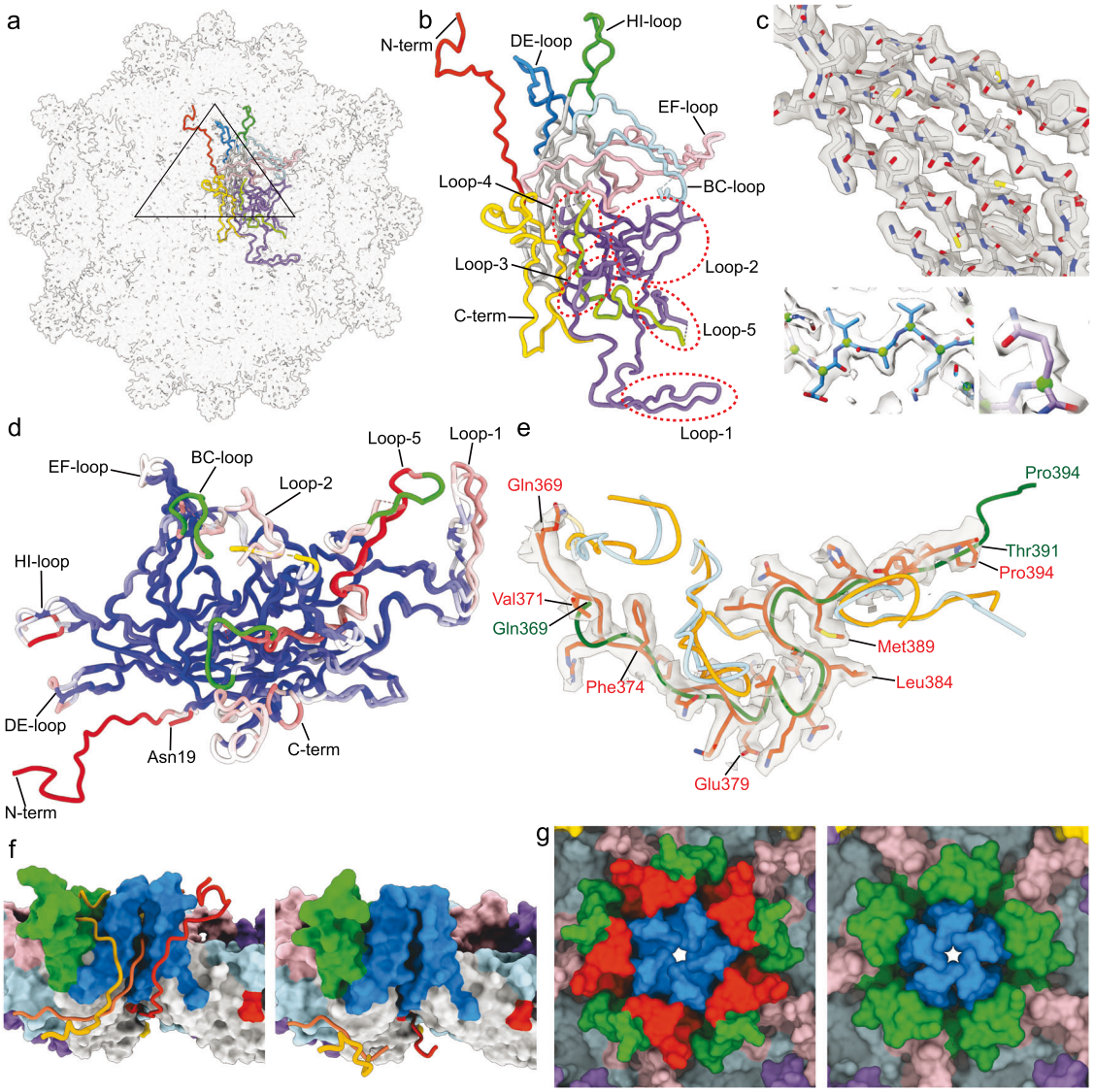

Fig. 2 | Atomic model of the authentic B19V revealed VP2 N-terminal residues extruding at the fivefold vertex. a, **b** Atomic model of the B19V VP2 protein depicted in a ribbon diagram. In the cryoEM map, the VP2 structure is displayed for an icosahedral asymmetric unit (black triangle) (**a**) with each surface loop uniquely colored and labeled (**b**). **c** The map and model quality are illustrated by the Cα backbone and side chains in the separated β-strand and representative residues (bottom: I126, V128, and Q440). **d** Superimposition of VP2 structures of B19V virion with the VLP (PDB ID: 1S58). Both structures are presented in licorice representation and color-coded by RMSD (from high value in red to low in blue). The N-terminus of VP2 (aa 2-18) absent in the VLP was built and highlighted in orange red in the virion. All surface loops absent in the B19V virion, but built in the VLP, are colored in green. **e** Zoom detail of the residues 369-394, depicted in ribbon a diagram. The B19V residues (orange) are shifted forward compared to VLP (green). The cryoEM density was displayed in a transparent envelope. **f** Surface rendering side views of the fivefold vertex are shown for three VP2s (virion: left and VLP: right), while the N-terminus of each symmetry related protein is shown in a licorice representation, distinguished by yellow, orange, and red-orange. The solid surfaces were colored as in (**b**). **g** comparison of the capsid surface features at the fivefold vertex. The zoomed top view highlights the disparity between the two topologies (virion: left and VLP: right), particularly the N-termini, since the first ordered residue of the VLP is Asn19. The solid surfaces were colored as in (**b**).

After particle picking and 2D classification (Fig. 1b), the selected particles were reconstructed with icosahedral symmetry imposed to produce the authentic B19V virion map at a resolution of 2.2 Å (Fig. 1c–e), as determined by Fourier Shell Correlation at 0.143 cutoff (Supplementary Table 1 and Supplementary Fig. 1). The inside of the capsid was densely filled with the symmetry-averaged DNA genome. Outside the capsid, the extending densities protruded from the icosahedral twofold. The density magnitude of the protrusions was similar to that of the capsid (C. 1c). In addition to the extra densities on the twofold axis, the surface topology was different from the VLP structure (Fig. 1d)[11]. Compared to the VLPs, the B19V virion had a broader cylindrical fivefold, the threefold protrusions were less prominent, and the canyon encompassing the fivefold vertex was narrower (Fig. 1d). The depressions along the twofold axes were occluded by the extending proteinaceous densities, which were more apparent at lower contour levels (Fig. 1e). These densities are consistent with proteins asymmetrically bound across the symmetry axis.

Atomic structure of the native B19V capsid

For de novo model building, ModelAngelo[26] was used with the B19V VP2 sequence (UniProt access code: Q76T42). The de novo model was subsequently refined against our cryoEM map (Fig. 2a)[11]. The final structure had a predicted and actual Q score of 0.7274 and 0.84, respectively, indicating the validity of the refined B19V structure[27]. Atomic coordinates for the majority of VP2 residues spanning from Thr2 to Leu554 were confidently assigned without ambiguity

(Fig. 2b, c). However, certain residues located within surface loops, including the residues 63-72 (BC-loop), 303-311 (loop-2), 359-368 (loop-4), and 395-401 (loop-5), were not built due to local regions of weak density, suggesting flexibility (Fig. 2d). Within the VP2 structure, the characteristic jelly-roll motif emerged, comprising an eight-stranded antiparallel β-barrel interconnected by loops that shape the surface features (Fig. 2b). The extra density at the twofold axes remained unfilled and did not correspond to any of the B19V VP2 residues.

Comparison of the atomic models between the B19 virion and the VP2-VLP revealed a high similarity overall with a root-mean-square deviation (RMSD) of 3.00 Å (Fig. 2d). However, the analysis also underscored significant distinctions between the two structures:

(1) The virion included more disordered surface loops, with four loops being disordered in the virion (as listed above). In comparison, only one surface loop (residues 301-313, loop-2) was disordered in the VLP and the other three VLP loop structures were resolved, but with high B-factors (>165 $Å^2$)[11]. The enhanced flexibility observed in the virion surface loops might arise from variations in capsid composition (including the encapsidated genome), environmental factors (such as solution vs crystal conditions), or other contributing factors.

(2) A significant difference was observed in the long polypeptide chain (residues 369-394), which connect the two disordered loops (loop-4 and -5) in the virion (Fig. 2d, e). The 369-394 loop structure is conserved between the virion and VLP; however, the peptide chain is shifted by 2 to 3 residues in the superimposition. Although the superimposition suggests different residue locations (Fig. 2e), the possibility of error in the VLP model residue assignment due to the moderate resolution could not be ruled out[11]. Two adjacent loops (loop-1 and 2) from the two threefold symmetry-related VP2s showed higher RMSD values, likely due to adjustments necessitated by the residue shifts (Fig. 2d and Supplementary Fig. 2).

(3) Additionally, the native B19V capsid structure revealed the N-terminus of VP2 (residues 2-19), which protruded to the exterior of the capsid. In contrast, the most N-terminal ordered VP2 residue in the VLP was Asn19[11], situated underneath the capsid shell (Fig. 2f). The disparity in VP2 N-terminal extension of the virion resulted in a significant conformational difference around the fivefold vertex compared to the VLP (Fig. 2g). Specifically, the residues preceding the β-strand A (VP2 19-21) were anchored to the capsid shell, while the same residues were distal from the capsid shell in VLP. Then, the Glycine-rich motif (GAGGGG, VP2 12-17) threaded between symmetry-related DE-loops around the fivefold β-cylinder (residues 133-139, RMSD of 4.042 Å) (Fig. 2f). Our atomic structure of the N-terminus of VP2 corroborated the predicted model derived from the low-resolution difference map comparing B19V and VP2-VLP[22].

Subvolume analysis of the non-viral density on the twofold axes

The non-virus globular density that was consistently observed across original micrographs and in the 2D classes mapped to the B19V icosahedral twofold axes (Fig. 1a, b). The density exhibited secondary structural features of a protein, had strong central density above the axis, and weaker density magnitude at the periphery compared to the capsid (Fig. 1c–e). These features describe a protein bound asymmetrically across the twofold axis with partial occupancy due to steric clash between symmetry-related molecules. To characterize the extra density, subparticles were extracted and classified, designating volumes that completely encompassed the unknown twofold densities (Supplementary Fig. 3)[28]. The 60 subvolumes were classified without symmetry or alignments, which revealed that the binding mode for the unknown protein stretched across the twofold axis (Fig. 3a). Thus, only one molecule could bind at each icosahedral twofold axis. An occupancy analysis agreed with the observation of steric occlusion, finding that about 23 molecules were bound per capsid (38.3% of the sixty binding sites) (Fig. 3a). The 3D classified orientations allowed us to reconstruct the whole capsid with only one ligand bound to better resolve the protein at the twofold of the B19V capsid (Fig. 3b).

A second protein density discovered at the fivefold vertex

While processing the subvolumes designated to explore the twofold density, an additional proteinaceous density was discovered. This separate density was bound in proximity to the icosahedral fivefold axis (Supplementary Fig. 3). Initially, to explore this new density, subparticles were extracted from each fivefold vertex. 3D classification of this broad search showed symmetry-related densities around the fivefold axis (Supplementary Fig. 3). Using this result, 60 new subparticles were designated with a center focused on one of the fivefold densities. The subsequent 3D classification improved the density quality and revealed that there was about one molecule bound per fivefold vertex (19.4% of the sixty binding sites) (Fig. 3c). The resulting asymmetric 3D map of the virion-protein complex reconstructed a single copy of the molecule attached at the fivefold vertex, leaning across the capsid surface, and extending toward the twofold axis (Fig. 3d). In this complex map, the adjacent twofold binding density was not averaged out but had the opposing orientation from the previous result (Fig. 3b, d), indicating steric clash between the fivefold and twofold molecules within the same icosahedral asymmetric unit. The fivefold binding density exhibited diminished intensity compared to the capsid, gradually weakening with increasing distance from the capsid. Further examination of the classified subvolume map revealed an additional density extending from one side of the unknown fivefold density at a lower contour level (Fig. 3c, bottom right), suggesting a molecular flexibility.

Acute-phase reactants serpinA3 and ITIH4 bound to the B19V virion

To identify the proteins occupying the unfilled densities at the twofold and fivefold, SDS-PAGE and mass spectrometry (MS) analysis of purified B19V samples were performed. SDS-PAGE revealed an unknown 130 kDa protein migrating in addition to VP1 (83 kDa) and VP2 (58 kDa) capsid protein monomers (Supplementary Fig. 4a, b). MS identified inter-alpha trypsin inhibitor heavy chain 4 (ITIH4) from this band (Supplementary Fig. 4c). ITIs (inter-α-trypsin inhibitors) are a family of plasma protease inhibitors that contribute to extracellular matrix stability by covalent linkage to hyaluronan[29]. ITIs are assembled from a light chain and five homologous heavy chains (encoded by ITIH1 to ITIH5). As there is no structure for ITIH4, the closely related homologous protein, ITIH1 (PDB ID: 6FPY)[30], was used to interpret the two unknown densities. The homologous model was fitted into the extra density on the fivefold axis with a correlation coefficient of 0.5.

MS also revealed another protein, serpinA3, within the band corresponding to VP2 (Supplementary Fig. 4c). The molecular weight of serpinA3 is similar to that of B19 VP2 (~55–66 kDa vs 58 kDa), which allowed the proteins to co-migrate. Serpins (from serine protease inhibitors) are a superfamily of proteins that have protease inhibition activity and are found in all kingdoms of life. The atomic model of native serpinA3 (PDB ID 6HGE) was fitted into the corresponding cryoEM density at the twofold axis, which yielded a correlation coefficient of 0.71[31]. The MS results were confirmed by immunoprecipitation, in which virions were captured by ITIH4- and serpinA3-specific antibodies with an efficiency similar to that of a B19V-specific antibody against intact capsids (Caps; 860-55D)[32] (Supplementary Fig. 4d).

SerpinA3 and ITIH4 are bound to B19V in all plasma samples tested

To understand whether the structural configuration of B19V shielded by host proteins is a common or rare occurrence, nine additional de-identified B19V-infected plasma donations were tested (Supplementary Table 2). Virions from the different plasma samples were immunoprecipitated with antibodies against B19V capsid, ITIH4, and

https://doi.org/10.1038/s41467-024-53794-1

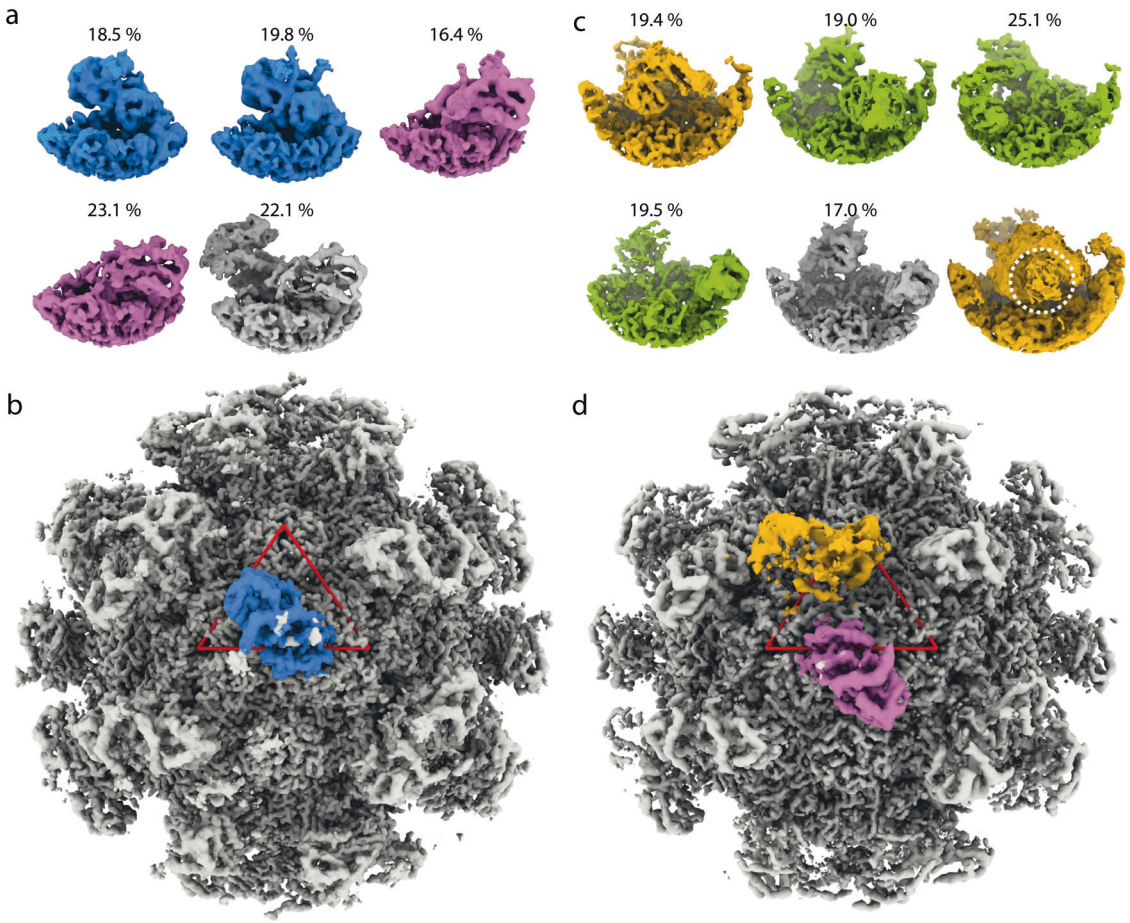

Fig. 3 | Subvolume analysis identified two extra densities protruding from the B19V capsid surface at the icosahedral twofold and fivefold axes. a 3D classification result of the subparticle images focusing on the twofold axis. Two classes (depicted in light blue) revealed the presence of an unknown molecule bound with the same upward orientation at the twofold, while another class (represented in pink) consist of the same molecule but bound with different downward facing orientation at the twofold symmetry-related site. **b** The light blue classes from (**a**) were combined and used to reconstruct an asymmetric map of the complex with one of the unknown densities colored in blue within the asymmetric unit (red triangle at a radius of 130 Å). **c** 3D classification results of subparticles around the fivefold axis. One class (colored in gold) displayed a bound molecule around the fivefold symmetry axis, while three classes (depicted in green) revealed three symmetry-related molecules. At the bottom right, the gold-colored class was shown at a lower contour to illustrate an extra density domain extending from side (dotted white circle). **d** The particles for the gold-colored class were employed to reconstruct the asymmetric map of the complex shown in gray with one fivefold density (gold) and the unknown twofold density (pink) shown in the downward orientation.

serpinA3 and quantified by qPCR. Without exception, both proteins were found bound to the virus (Fig. 4a, b).

One of the infected plasma donations corresponded to genotype 2, which is recognized as an ancient genotype and rarely identified as a circulating virus. The buoyant density of a genotype 1 virus (plasma donation P1; virus used for cryoEM) was compared with that of genotype 2 (plasma donation P10) by iodixanol gradient ultracentrifugation. Both viruses exhibited a single density peak of 1.21 g/ml, indicating that the average number of host proteases bound per capsid remained consistent between the two genotypes (Fig. 4c). The presence of the bound host PIs effectively increased the diameter of the virus by approximately 8 nm (Fig. 1e), resulting in the density of native B19V being significantly lower than that observed for other parvoviruses, 1.26–1.30 g/ml[33,34].

Plasma samples from three patients consisted of serial donations corresponding to pre-viremia, peak of viremia, IgM + /IgG-, and IgM-/IgG + . Plasma P8 included an additional donation at the onset of viremia (ramp-up) (Fig. 4d) (Supplementary Table 2). B19V from plasma P8 was immunoprecipitated with ITIH4 and serpinA3 antibodies at all viremic phases (Fig. 4e). The viral particles exhibited identical density profiles, except when bound to IgM, whereby the binding of the bulky immunoglobulin resulted in a reduced density (Fig. 4f). These findings suggest that throughout a natural infection, irrespective of the viremic phase or genotype, B19V circulates in the blood plasma coated by the two host protease inhibitors.

Structures of serpinA3 and ITIH4 bound to B19V capsid

Serpins irreversibly inhibit their target proteases by a mousetrap-like mechanism. When a protease binds and cleaves the recognition site in the reactive center loop (RCL), the serpin undergoes a dramatic conformational change resulting in the "trapping" of the covalently bound protease and the inactivation of both, the serpin and the protease[35]. Serpins exhibit distinct conformation states, including native (uncleaved) and cleaved states, determined by the conformations of the RCL and the number of β-strands of the β-sheet A (Fig. 5a). To identify the state of the bound serpin, a fitting analysis was done using crystal structures of both native and cleaved serpin conformations. The fitting results affirmed that the serpinA3 bound to B19V assumed the native state, characterized by an uncleaved flexible RCL and the four-stranded β-sheet A. The local resolution of the serpin density in the asymmetric map of the B19V-serpinA3 complex ranged from 3.5 to 5.5 Å (Fig. 3b and Supplementary Fig. 5a, b). Therefore, prior to model

https://doi.org/10.1038/s41467-024-53794-1

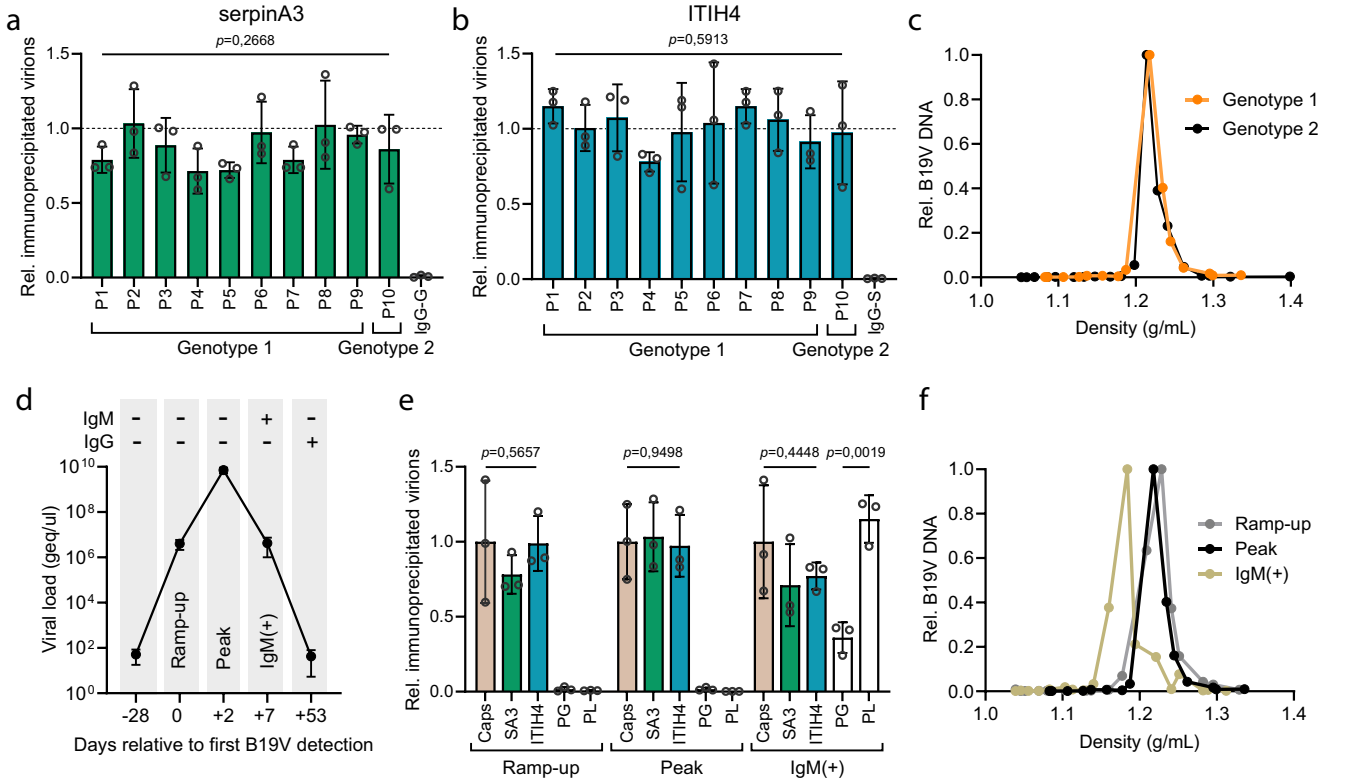

Fig. 4 | Infectious B19V isolated from human plasma is bound to ITIH4 and serpinA3 in all individuals tested and at different viremic phases. **a**, **b** Immunoprecipitation of B19V from different plasma donations (P1 to P10) with antibodies against intact capsids (860-55D), ITIH4, or serpinA3. DNA from immunoprecipitated virions was quantified by qPCR ($n = 3$). The values shown represent the proportion of immunoprecipitated virions relative to the total virions (immunoprecipitated with the antibody against intact capsids; dotted line). As negative controls, IgGs from the host species used to raise serpinA3 (goat) and ITIH4 (sheep) antibodies were used without the primary antibody. IgG-S, sheep IgG; IgG-G, goat IgG. **c** Iodixanol density gradient ultracentrifugation of plasma P1 (genotype 1), and plasma P10 (genotype 2). **d** Evolution of viremia (B19V geq/µl) and humoral immune response (IgM/IgG) in one donor (plasma P8). **e** Immunoprecipitation of B19V from plasma P8 with antibodies against intact capsids, ITIH4, or serpinA3 at day 0 (ramp-up), day 2 (peak), and day 7 (IgM + /IgG-). Viral DNA was quantified from immunoprecipitated samples. As controls, samples were immunoprecipitated with protein G (PG) or protein L (PL) alone ($n = 3$). **f** Iodixanol density gradient ultracentrifugation of plasma P8 at day 0 (ramp-up), day 2 (peak) and day 7 (IgM + / IgG-). Data in (**a**, **b**, **e**) are presented as the mean ± SD of three biologically independent experiments and compared using one-way ANOVA test.

building of the bound serpinA3, local refinement of the subvolume was performed to improve the map. The refined subvolume exhibited a local resolution range between 3.0 Å and 3.4 Å (Supplementary Fig. 5c), which was used to build the atomic model. The subvolume also revealed five extra densities that corresponded to the predicted N-glycosylation sites of serpinA3 (Supplementary Fig. 5d), a key characteristic of plasma-derived serpins[36]. The atomic structure of the B19V-bound serpinA3 superimposed with the active serpin crystallographic structure (PDB ID 6HGE)[31] with a RMSD of 1.156 Å and had similar disordered peptides for the flexible RCL (residues 351-366).

The ITI heavy chains are composed of three distinct domains[29]: a single von Willebrand factor type A (vWFA) domain, in which a metal ion-dependent adhesion site (MIDAS) motif is located; an integrin-like hybrid domain (HC-Hybrid1); and another HC-Hybrid2 domain (Fig. 5b). Unlike other family members, the active form of ITIH4 includes a unique C-terminal region that contains a proline-rich region (PRR), which includes protease-susceptible region, and a tectonin-like β-propeller repeat[37]. ITIH4 structure was predicted by using SWISS-MODEL and AlphaFold2[38,39]. Whereas SWISS-MODEL generated a model containing only the family-shared domains, AlphaFold2 predicted a structure with complete domains, including the β-propeller repeat (Supplementary Fig. 6a, b) (AlphaFold2 entry: Q14624). AlphaFold2 also identified long disordered residues spanning 621-733, which connect the Hybrid2 and β-propeller domains and include the PRR region (Supplementary Fig. 6b). The ITIH4 density in the asymmetric complex map showed a similar local resolution range as serpinA3, but the density quality was poorer than that of the serpinA3 (Supplementary Fig. 6c, d). Although the subvolume was refined using a similar approach to that containing SerpinA3, the resulting ITIH4 density was not sufficient for atomic model building, likely due to the noisy data and fewer particles (Supplementary Table 1). Instead, the ITIH4 homology model was fitted into the fivefold density. The fit yielded the correlation coefficient value of 0.4939 (Fig. 5b). The vWFA domain fit well into a region of continuous, complete cryo-EM density located directly adjacent to the capsid surface. More distal from the binding interface, the density for the hybrid domains became weaker, suggesting less rigid conformation or flexible binding. Notably, the β-propeller repeat structure fitted within the weakest density observed at lower contour level (Fig. 3c, Supplementary Fig. 6e, f), suggesting that the ITIH4 on the capsid is in a pre-cleavage state. Thus, both serpinA3 and ITIH4 binding to the B19V capsid had enzymatically active forms.

After the local refinement, the ITIH4 subvolume density map revealed additional, proteinaceous unfilled density in the depression around the fivefold vertex beneath and adjacent to the bound ITIH4 (Supplementary Fig. 7a). Using ModelAngelo[26] with VP1, serpinA3, and ITIH4 input as reference sequences, a portion of the density was identified as RPGVLSSRQ. This sequence corresponded to the ITIH4 residues 661-669 within the missing loop in AlphaFold2 model (Supplementary Fig. 7b).

https://doi.org/10.1038/s41467-024-53794-1

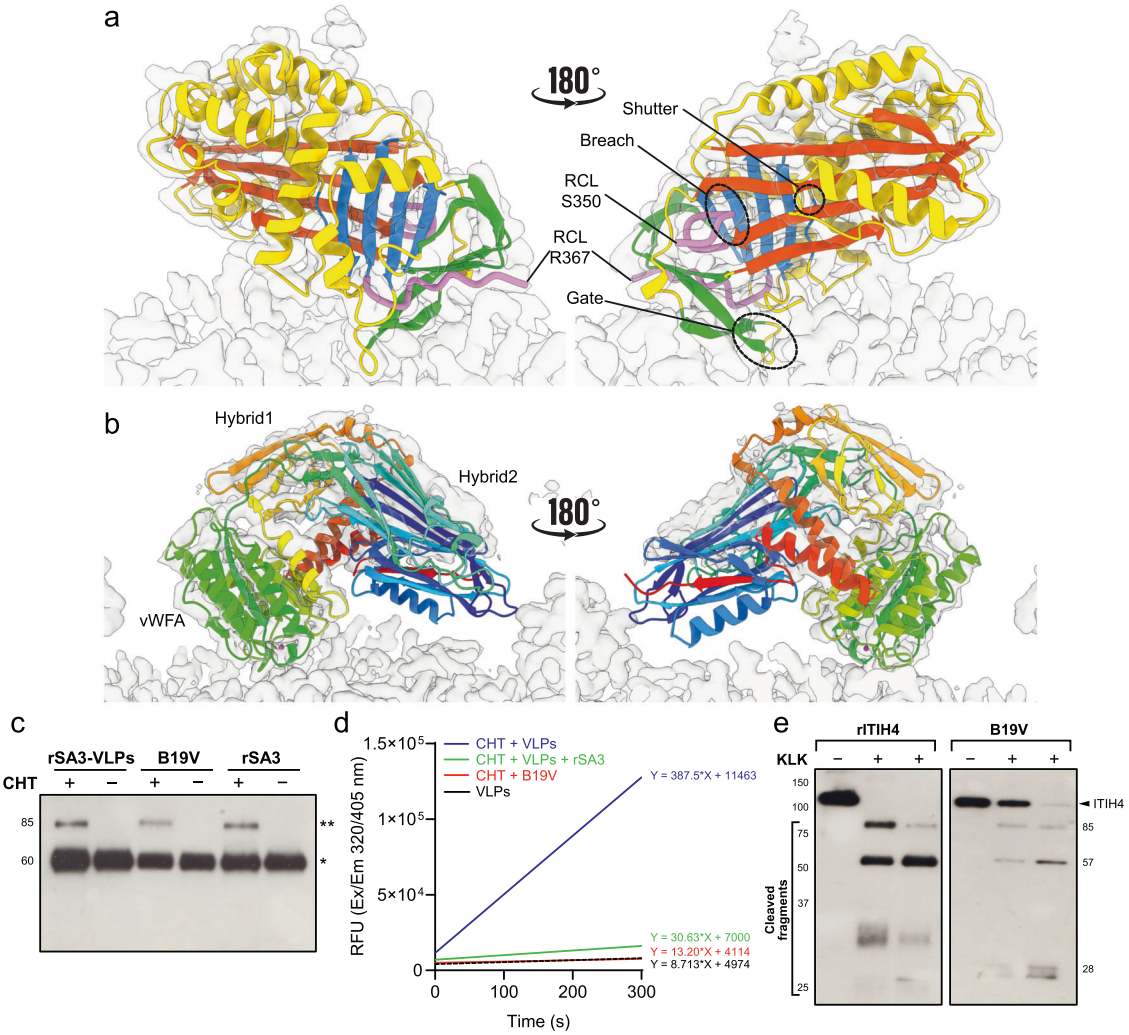

Fig. 5 | SerpinA3 and ITIH4 bind the capsid, exposing the active site, and retaining their native activity, conferring protease inhibitory properties to the virions. a Atomic structure of B19V-bound serpinA3, shown as a ribbon diagram, rotated by 180° around the twofold axis, with β-sheets A, B, and C shown in red, blue, and green, respectively. Part of the reactive center loop comprised of residues from 343 to 350 are shown in pink. The shutter, breach, and gate domains are labeled (dotted circles), the two terminal residues ordered and built for the reactive center loop (RCL) are indicated. **b** A homology model of ITIH4 was fitted into the cryoEM density on the fivefold vertex. ITIH4 contains a von Willebrand Factor A (labeled vWFa) domain with a metal-ion dependent adhesion site motif and associated hybrid domains. The ribbon diagram was colored for each chain in rainbow color successively (blue to red) from N- to C-terminus. Hybrid 1 and 2 domains are labeled. **c** Formation of covalent complexes between chymotrypsin (CHT) and serpinA3 (SA3). Purified B19V particles, recombinant serpinA3 (rSA3), and rSA3 in the presence of virus-like particles (VLPs) were incubated at 37 °C for 30 min, using a molar SA3 to protease ratio of 20:1. Western blot was performed with an antibody against SA3. (*) SA3 monomer (60 kDa); (**) SA3-protease complex (85 kDa). **d** B19V inhibits chymotrypsin activity in vitro. Purified B19V, rSA3, and rSA3 in presence of VLPs were incubated with CHT (20:1). The mixtures were then incubated with a fluorogenic peptide and the RFU was measured at excitation and emission wavelengths of 320 and 405 nm, respectively, for 5 min. **e** Capsid-bound ITIH4 is cleaved by kallikrein (KLK) in vitro. Purified B19V or recombinant ITIH4 (rITIH4) was incubated with activated plasma kallikrein for 4 and 6 h, at 37 °C, using an ITIH4 to protease ratio of 20:1. Western blot was performed with an antibody against ITIH4. ITIH4 monomer corresponds to the 120 kDa band. Experiments in (**c**, **e**) were repeated three times independently with similar results. Molecular weight is shown (kDa).

Functional characterization of serpinA3 and ITIH4 bound to B19V

In the B19V-serpinA3 complex structure, the protease cleavage site in the RCL is accessible (Fig. 5a), suggesting that serpinA3 maintain active enzyme function while bound to the capsid. To test the activity of the capsid-bound serpinA3, an in vitro activity assay was performed. Purified B19V was incubated with α-chymotrypsin, and the formation of covalent suicide complexes was assessed by Western blot. The integrity of the capsids was assessed by immunoprecipitation with an antibody against intact capsids (860-55D) (Supplementary Fig. 8a). Capsid-bound serpinA3 formed covalent complexes with the protease that were comparable in size and quantity to those formed with recombinant serpinA3 alone or in the presence of B19V VLPs (Fig. 5c). To further validate the activity of the capsid-bound serpinA3, a chymotrypsin activity fluorometric assay was performed to detect the protease inhibitory activity of B19V purified from plasma. Recombinant human serpinA3 and B19V VLPs were used as a positive and negative controls, respectively. Incubation of chymotrypsin with purified B19V resulted in inhibition of protease activity similar to that observed with recombinant serpinA3 (Fig. 5d).

Unlike serpinA3, ITIH4 is cleaved within the protease-susceptible region (PSR) by kallikrein and other proteases. The cleaved peptides can form non-covalent complexes with the executing protease to inhibit its activity[37]. To investigate whether kallikrein can access the PSR and cleave ITIH4 bound to B19V capsids, purified B19V and recombinant human ITIH4 were incubated with activated plasma

https://doi.org/10.1038/s41467-024-53794-1

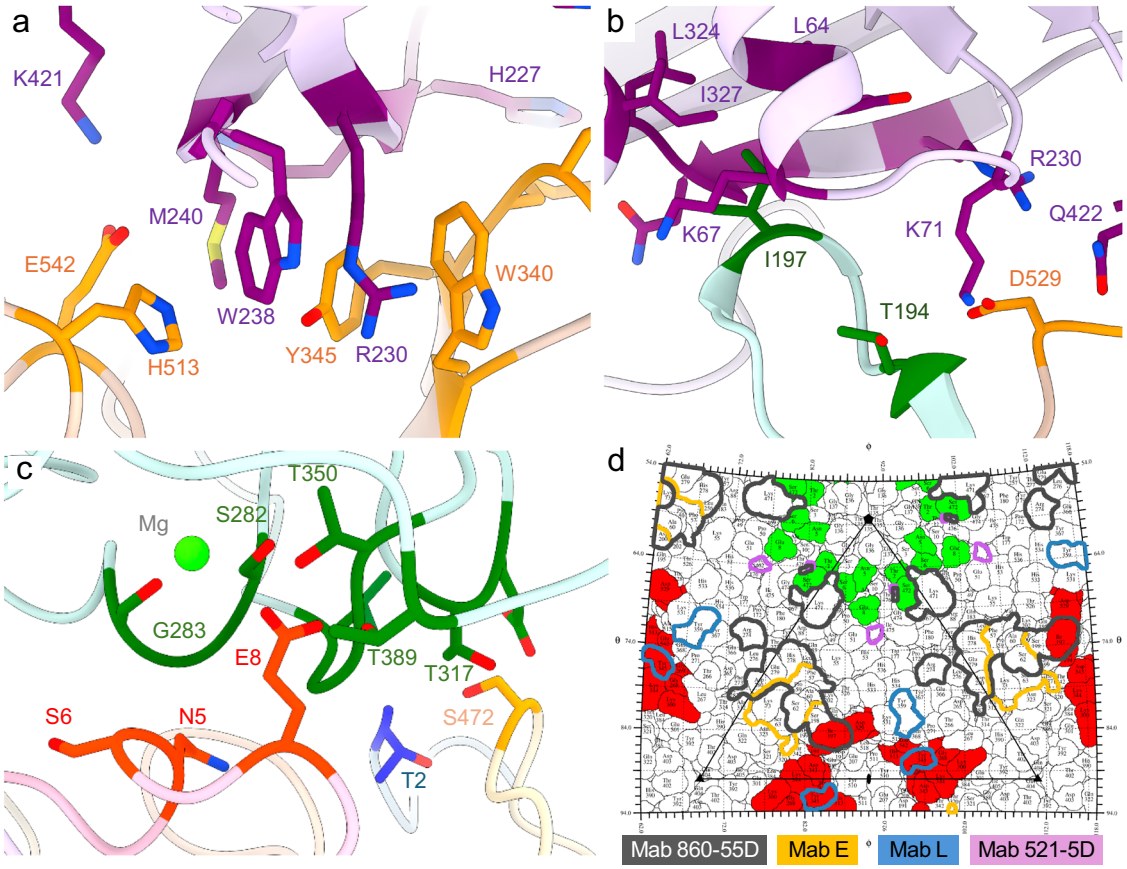

Fig. 6 | Molecular interactions between B19V and PIs. To minimize clash and identify contacts, the serpin model and ITIH4 homology model were refined with the six and five VP2 molecules, respectively within the footprints. **a**, **b** Molecular interactions between serpinA3 and B19V. The contacts in the eastern (**a**) and northern area (**b**) of the twofold depression of B19V are shown (Supplementary Fig. 7). In eastern region, VP2s interact with the serpinA3 β-sheet C (**a**), while in the northern region, they interact with the β-sheet A and adjacent α-helix (**b**). Molecules are depicted as ribbon diagrams, with contacting residues displayed as stick models and labeled accordingly. Contacts on the SerpinA3 are highlighted in purple, while the two VP2s are colored in orange and green, respectively. **c** Contacts between ITIH4 and B19V. The fitted ITIH4 homology model (green) and VP2s (red, blue, and orange) are depicted as licorice diagrams. Contacting residues are shown as stick models and labeled accordingly. The superimposed magnesium ion is represented as a green sphere. **d** Overlap of the PI footprints and antigenic sites. The footprints of the serpinA3 (red) and ITIH4 (green), along with antigenic sites of the four neutralizing antibodies (color-marked as per the key), are displayed on the road map of B19V capsid surface[41].

kallikrein. The integrity of the capsids incubated with kallikrein was assessed by immunoprecipitation with an antibody against intact capsids (860-55D) (Supplementary Fig. 8b). As shown in Fig. 5e, kallikrein cleaved capsid-bound ITIH4, albeit at a slower rate compared to recombinant ITIH4. Thus, the structural and functional evidence indicate that capsid-bound serpinA3 and ITIH4 retain their native activity, conferring host protease inhibitory properties to the virions.

Molecular interactions of serpinA3 and ITIH4 with the B19V capsid

To elucidate the molecular interactions between the B19V capsid and the two proteinases, the contact residues at the interface were identified (Fig. 6). The refined serpinA3 structure was placed into the complex map in its native conformation bound to B19V capsid (Fig. 5a) and re-refined with the six VP2 molecules in the footprint to minimize clash and identify contacts. This second round refinement into slightly lower resolution density map did not affect the structures, yielding Cα-RMSD values of 0.326 and 0.191–0.383 Å between before/after the refinement of the serpin and six VP2 chains, respectively. The serpinA3 gate region along with the β-sheet C extended into the twofold depression of the B19V capsid (Fig. 5a), interacting with VP2 residues on the GH-loops and carboxy-terminus (Fig. 6a). Additionally, serpinA3 β-sheet A and α-helix A as well as the RCL C-terminus interacted with the capsid residues on VP2 EF- and GH-loops (Fig. 6b). The serpinA3 footprint included multiple surface loops around the twofold axis formed by four copies of VP2, specifically binding one VP2 Ile197 and an additional VP2 Ile197 related by twofold symmetry (Supplementary Fig. 9a) (Supplementary Table 3). The diagonal orientation and position of the ligand over the twofold axis resulted in asymmetric interactions, explaining why only one serpinA3 molecule can bind each icosahedral twofold.

The identification of the ITIH4 footprint was performed by fitting the vWFA domain (residues 271-459) separately into the cryoEM density of the corresponding asymmetric map to improve the fitting (cross correlation 0.5595). Examining the footprint of the ITIH4 revealed only five contact residues on the B19V capsid surface (Fig. 6c) (Supplementary Fig. 9b) (Supplementary Table 3). It should be noted that when the full homology model was fitted into the cryoEM map, additional contacts were found between the ITIH4 hybrid2 domain and VP2s, however, those were excluded as there is no cryoEM density supporting the model (Fig. 5b). Among the five residues, four mapped onto the VP2 N-termini adjacent to the fivefold pore, and three of them belonged to a single VP2 (Supplementary Fig. 9b) (Supplementary Table 3), indicating the VP2 N-terminus is crucial for binding to ITIH4 (Fig. 6c). Additional contact occurred with Ser472 from an adjacent HI Loop. When ITIH1 crystal structure (PDB ID: 6FPY)[30] was superimposed, the magnesium metal ion within the MIDAS domain was positioned in close proximity to the sidechain of Glu8, suggesting a

https://doi.org/10.1038/s41467-024-53794-1

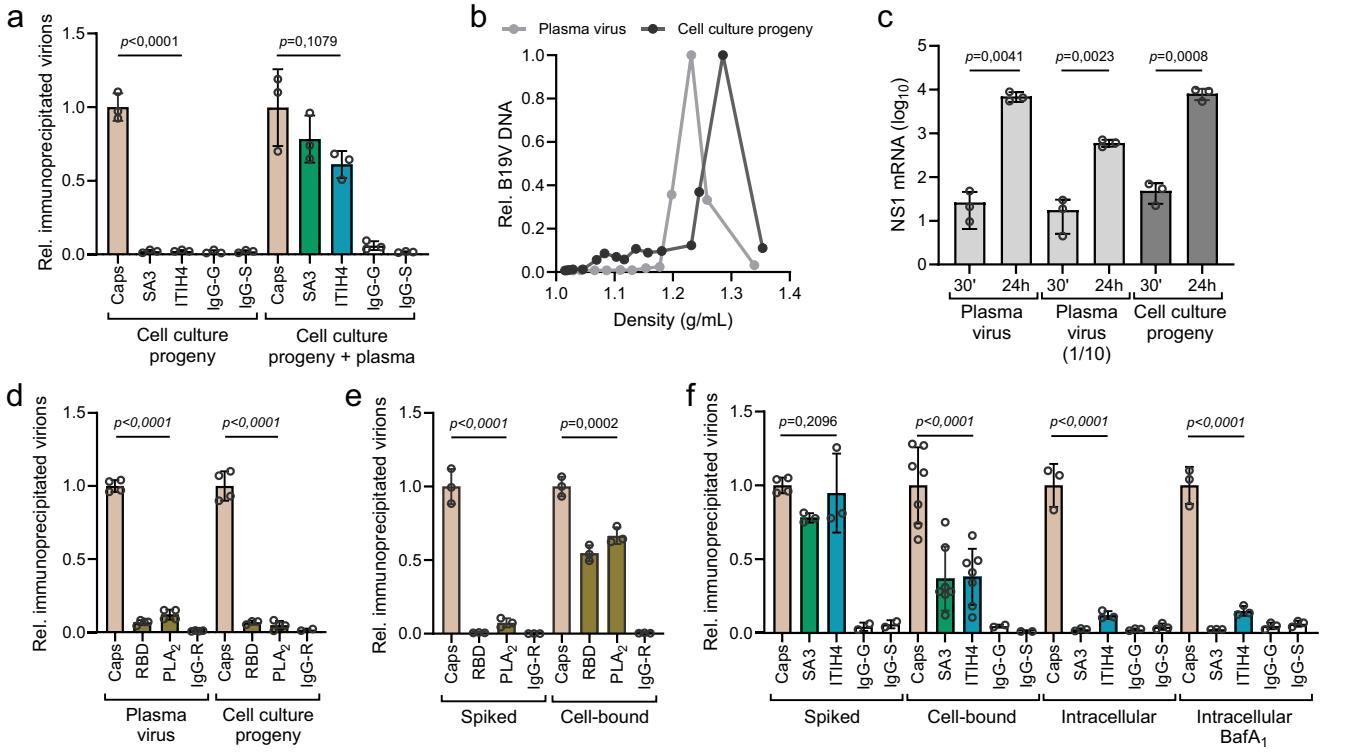

Fig. 7 | Protein-coated virions remain infectious as PIs dissociate from the capsid before entry. a ITIH4 and serpinA3 bind to cell culture-derived virions incubated with human plasma. EPCs were infected with B19V under hypoxic conditions. After 72 h, progeny virions in the supernatant were incubated with PBS or with plasma devoid of B19V and B19V-specific antibodies, at 100-fold dilution for 1 h at 37 °C. Virions were immunoprecipitated with antibodies against intact capsids (Caps), SA3 and ITIH4. Viral DNA from immunoprecipitated capsids was quantified by qPCR ($n = 3$). **b** Iodixanol density gradient ultracentrifugation of virions from plasma or cell culture. **c** UT7/Epo cells were infected with equal amounts of plasma and progeny virions obtained from the iodixanol peak fractions. As a control, B19V infected plasma was 10-fold diluted. B19V NS1 mRNA was quantified by RT-qPCR at 30 min (input) and 24 h post-infection ($n = 3$). **d** Accessibility of VP1u. Virions from plasma or cell culture were immunoprecipitated with an antibody against intact capsids (Caps), and antibodies against VP1u (receptor-binding domain (RBD) and phospholipase A2 (PLA2) regions). Viral DNA from immunoprecipitated capsids was quantified by qPCR ($n = 4$, $n = 3$ for RBD plasma virus). **e** Externalization of VP1u upon interaction with host cells. Spiked: virus incubated with lysed cells. Cell-bound: virus incubated with cells at 4 °C. Cells were washed, lysed, and capsids were immunoprecipitated with the indicated antibodies. Viral DNA was quantified from immunoprecipitated capsids by qPCR ($n = 3$). **f** Dissociation of serpinA3 and ITIH4 from capsids upon interaction with host cells. Spiked: virus incubated with lysed cells. Cell-bound: virus incubated with cells at 4 °C. Intracellular: virus incubated with cells at 37 °C for 30 min in untreated and bafilomycin A1-treated cells. For all conditions, cells were washed, lysed, and capsids were immunoprecipitated with antibodies against intact capsids (Caps), serpinA3 (SA3), and ITIH4. Viral DNA was quantified from immunoprecipitated capsids by qPCR ($n = 4$ for Caps spiked, $n = 7$ for Cell-bound, $n = 3$ for the rest). All samples are biologically independent samples. Statistical significance was calculated using two-sided Student's t test (**c**) and one-way ANOVA with multiple comparisons (**a**) and (**d**–**f**). The results are presented as the mean ± SD of three or more independent experiments.

potential role of the metal ion in the B19V-ITIH4 interaction (Fig. 6c). All these contact points clustered together at a single position on top of the fivefold vertex, and thus serve as a very narrow point of contact for ITIH4 (Supplementary Fig. 9b). These limited contacts would cause a swaying motion of the ITIH4, corroborating with the weaker density of the distal domains away from the interaction site[40].

SerpinA3 and ITIH4 footprints overlap known antigenic epitopes

SerpinA3 and ITIH4 footprints were plotted to the B19V surface using a roadmap, which is a stereographic projection of the surface of the virus[41]. The known antigenic sites on the virus (Fig. 6d), described by four antibodies known to neutralize B19V (Mab 860-55D)[18] or inhibit hemagglutination of B19V (Mab E, L, and 521-5D)[14–17] were also plotted to the same roadmap. Among the four, three antibodies (Mab 860-55D, E, and L) had footprints overlapping or touching the footprint of serpinA3. The footprint of the two monoclonal antibodies (Mab 860-55D and 521-5D) were overlapping or adjacent to that of ITIH4 (Fig. 6d). When the cryoEM densities of the two protease inhibitors were projected to the roadmap of the four antibodies, it was more evident that the capsid-bound proteins would obstruct binding of those antibodies (Supplementary Fig. 9c, d). Especially, the bulky ITIH4 density covered the parts of all four antibody footprints within the asymmetric unit (Supplementary Fig. 9d). It should be noted that the efficacy of antibody blocking by the two host proteins, may vary depending on their occupancy and the binding orientation of serpinA3.

The virions with bound protease inhibitors remain infectious in cell culture

To test the ability of the protein-coated virions to enter and infect permissive cells, virus progeny was generated by infecting erythroid progenitor cells under hypoxic conditions[42] (Supplementary Fig. 10a, b). To characterize the progeny virion, immunoprecipitation demonstrated that virions produced in cell culture did not have host PIs bound. However, when the virions were incubated with uninfected human plasma, ITIH4 and serpinA3 bound to the capsids (Fig. 7a). Compared to B19V purified from patient samples, the progeny virions sedimented at a higher buoyant density (Fig. 7b). Infectivity assays, comparing the plasma-purified B19V virions with the cell culture progeny showed no significant difference. Both virus preparations were equally infectious, indicating that the binding of host PIs does not

interfere with virus entry and infection (Fig. 7c) (Supplementary Fig. 10c).

Dissociation of the host protease inhibitors

To understand the lack of interference by the bound PIs on virus entry, the capsid conformational change known to occur upon B19V interaction with the host cell—leading to the essential externalization of the VP1u[12,13]—was first examined. By using two antibodies targeting the two critical motifs in the VP1u, the RBD and the PLA_2, the internal and inaccessible position of VP1u in both plasma-derived and cell culture progeny virions was confirmed (Fig. 7d). It was also confirmed that interaction of the plasma-derived virus with UT7/Epo cells induced the capsid rearrangement leading to the externalization of VP1u (Fig. 7e). Then it was examined whether this capsid rearrangement affected the binding of the host proteins. B19V was incubated with UT7/Epo cells at 4°C to facilitate attachment to the cells without internalization; at 37 °C for 30 minutes to enable both virus attachment and internalization; and at 37 °C for 30 min in bafilomycin A1-treated cells to allow virus internalization in the absence of endosomal acidification. Attachment at 4 °C resulted in a significant dissociation of the PIs. The dissociation increased when the cells were incubated at 37 °C, and the alkalinization of the endosomes by bafilomycin A1 did not prevent the dissociation, indicating that the acidic endosomal pH is not the trigger for the dissociation (Fig. 7f). This result indicates that the dissociation of the PIs starts at the cell surface, likely due to the capsid conformational rearrangement required to expose the VP1u. These findings are consistent with the observation that, despite the large capsid surface area occupied, the virion-bound host proteins do not interfere with virus entry.

Discussion

The two acute-phase proteins (PIs) bound to B19V were found in all of the ten infected plasma donations used in this study, which were collected over the past 20 years in the USA and Europe. Nine were genotype 1, which is the predominant circulating virus today. One virus was genotype 2, which circulated widely before being replaced by genotype 1 in the 1970s[43]. Today, genotype 2 is considered extinct[43], and is often observed persisting in the tissues of individuals born before 1960–1970[44]. The fact that B19V was found in complex with the host PIs in all plasma donations, including the extinct genotype 2, suggests that these virus-host protein interactions are conserved and evolutionarily favored.

In a previous study, B19V particles purified from patient samples contained both empty and genome-filled capsids, which resulted in 11.3 and 7.5 Å structures, respectively[22]. Neither the genome-filled nor the empty capsid map resolved any bound molecules on the capsid surface. In this study, genome-filled capsids were characterized and every sample tested had ITIH4 and serpinA3 bound. The key differences between these two studies were that the previous purification protocol used CsCl gradients and included the presence of 25 mM EDTA. The use of CsCl as a gradient to purify B19V results in approximately 30% empty capsids[24], which did not bind ITIH4 and serpinA3. Since CsCl is hypertonic whereas iodixanol is isotonic, the purification protocol used here likely preserved the native virus architecture. Similarly, less EDTA was used to preserve potentially bound divalent cations essential for virus stability[23,45]. It is yet to be tested if the empty capsids (or procapsids) bind the host PIs, although it is likely that the procapsids have different PI-binding activities from VLPs as the externalized N-terminus is the main binding site for ITIH4.

An average of twelve ITIH4 molecules bound per capsid at the fivefold is consistent with one ITIH4 per vertex. The number of bound serpins (22 out of 30 sites occupied) compared to the number of ITIH4 (12 out of 12 sites occupied) suggests that it is ITIH4 that interferes with serpinA3 binding, not the alternative. Without a way to assess molecule affinity for the capsid, further speculation cannot be made.

Numerous viruses have evolved strategies to hide infection-relevant domains from immune surveillance. These strategies include conformational masking that restricts antibody access to occluded epitopes[46–48] and epitope shielding with host-derived glycans[49,50] or lipids[51]. Here, the overlap of protein binding and antibody footprints suggests that binding of host proteins hinders access to antigenic epitopes. Moreover, immune surveillance is likely hampered by the coating of the viral capsid with host proteins that are recognized as self. However, due to asymmetric interactions and steric interference between the binding of the two PIs, there is always partial exposure of a few antigenic epitopes per capsid, which was shown in our immunoprecipitation analysis using antibody 860-55D (Caps). Nevertheless, the specific binding of host PIs to the capsid may serve as an effective cloaking device, shielding the virus during circulation in the blood. This cloaking strategy may confer an advantage to the virus, explaining the remarkably high viremia levels unparalleled by any other viral infection, and the slower clearance of peripheral viremia despite the presence of specific IgGs[52–54]. Given the implications for transfusion medicine and fetal transmission, the reason for the remarkable high viremia and slow clearance of B19V has been the subject of active debate. While several factors may contribute, an intriguing explanation may be the ability of the virus to camouflage antigenic sites by coating the capsids with host plasma proteins.

The dissociation of the host PIs prior to viral uptake also suggests that their function is related to the extracellular viremic phase of the virus. If so, blood circulation of B19V shielded by host proteins and their dissociation prior to viral entry into erythroid progenitor cells appears to be a well-orchestrated strategy aimed at evading immune surveillance without compromising receptor interaction and entry. However, it is intriguing that the virus employs two structurally distinct host proteins that share the same function as protease inhibitors. To date, only large DNA viruses with substantial genetic resources, such as poxvirus, baculovirus, mimivirus, and megavirus have been shown to encode their own serpins. Virus-encoded serpins target diverse host proteases to modulate inflammatory responses and promote the infection. Although dispensable for virus replication in cell culture, viral-encoded serpins act as virulence factors in the context of a systemic infection, and their deletion reduces the lethality rates[55,56]. Serpins modulate a wide variety of biological processes, such as blood clotting, inflammation, immune-regulation, tumor-suppression, chromatin condensation, and apoptosis[57]. The ITIH4 is a poorly characterized plasma protein that targets multiple proteases, particularly those involved in intravascular host defense[37].

At present, it is challenging to directly associate the activity of the capsid-bound PIs to a specific extracellular function of the virus. Nevertheless, the acquisition of protease inhibition activity by the circulating virions implies their potential to exploit any of the diverse activities associated with serpinA3 or ITIH4. This activity may be important in protecting the circulating virus, notably the essential VP1u, from extracellular proteases, and/or in interfering with host defenses. For instance, plasma kallikrein is able to cleave C3 and activate complement. Inhibition of kallikrein by capsid-bound ITIH4 could impair C3 cleavage and stall the activation of complement antiviral activity[37,58]. SerpinA3 has been shown to inhibit cathepsin G secreted by neutrophils[59]. By cleaving extracellular matrix proteins and activating metalloproteinases, this protease contributes to neutrophil migration to the site of infection. Through its inhibition, B19V-bound serpinA3 could block neutrophil migration and its antiviral and pro-inflammatory effects in the bone marrow. The extent to which the virus exploits its protease inhibitory activity is currently unknown, and elucidation will likely reveal important aspects of B19V infection.

The consistent detection of B19V in complex with host PIs in both circulating and extinct viruses strongly suggests an evolutionary advantage for this interaction and highlights its relevance in systemic infection. This finding represents an additional facet of the interaction

between the virus and the host, and it is essential for understanding the pathogenesis of B19V. The use of patient-derived virus and subparticle analysis of the high-resolution structure were essential for the detection of the host proteins that coat the authentic, infectious B19 virions. This phenomenon would have been missed using conventional methods with cell culture-derived viruses, suggesting that binding of host proteins to viral capsids may have been overlooked and may be more common than previously thought.

Methods

Cells and viruses

The human megakaryoblastoid cell line UT7/Epo were cultured in Eagle's minimal essential medium (MEM) containing 5% fetal calf serum (FCS) and 2 U/ml recombinant erythropoietin (Epo). For erythroid differentiation, CD34+ bone marrow cells were expanded in alpha minimum essential media (αMEM) (Thermo Fisher Scientific, Waltham, MA) with 20% BIT 9500 (BSA, insulin, transferrin) (Stemcell Technologies, Vancouver, BC, Canada), 90 ng/mL ferric nitrate (Sigma-Aldrich, St. Louis, MO), 900 ng/mL ferrous sulfate (Sigma-Aldrich), 100 ng/mL stem cell factor (SCF) (Thermo Fisher Scientific), 5 ng/mL interleukin (IL)-3 (Thermo Fisher Scientific), 1 μM hydrocortisone (Sigma-Aldrich), and 3 U/mL rhEPO (EPREX®; Janssen-Cilag, Zug, Switzerland). For stem cell expansion, CD34+ cells were cultured for seven days in αMEM, 20% BIT 9500, supplemented with StemSpan CD34+ Expansion Supplement (10X) (Stemcell Technologies), containing the human growth factors FMS-like tyrosine kinase 3 ligand (Flt3L), SCF, IL-3, IL-6, and thrombopoietin (TPO). All cells were cultured at 37 °C and 5% CO_2.

De-identified plasma from B19V infected donors, with virus-specific serology and genotyping identification, were obtained from donations centers (CSL Behring AG, Bern, Switzerland). The de-identified samples do not require ethical approval. Plasma donation infected with genotype 2 was kindly provided by J. Blümel (Paul-Ehrlich Institute, Germany). Infected plasma samples were thawed and cleared by centrifugation at 1520 × *g* 4 °C for 10 min and virions were quantified by quantitative PCR (qPCR) using the iTaq™ SYBR® Green Supermix kit (Bio-Rad, Cressier, Switzerland) following the manufacturer's instructions. Plasmids containing the complete genome of B19V were used at 10-fold dilutions as external standards.

Purification and concentration of B19V from infected plasma

B19V was concentrated from a plasma donation (P1) by ultracentrifugation through a 20% sucrose cushion in PBS and 1 mM $MgCl_2$. The pellet was resuspended in PBS, 1 mM $MgCl_2$ and pelleted again through 20% sucrose. Viruses were further purified by iodixanol density gradient ultracentrifugation. Briefly, the virus suspension was applied onto an iodixanol gradient containing 2 mL 55%, 45%, 40%, 35%, and 15% iodixanol solution in PBS supplemented with 1 mM $MgCl_2$. The virus suspension was adjusted to 2 mL with the corresponding buffer and centrifuged at 245,000 × *g*, at 18 °C for 16 h in a swinging bucket rotor Beckman SW41Ti. After the centrifugation, 0.5 mL fractions were collected from the top. To determine the density of each fraction, the refractive index was measured using a refractometer. For each fraction, the presence of the virus was determined by qPCR, as described above. Positive fractions were pooled and analyzed by SDS-PAGE.

Antibodies and chemicals

The human monoclonal antibody (mAb) 860-55D against intact capsids was purchased from Mikrogen (Neuried, Germany). The rabbit polyclonal antibodies against the N-terminal (RBD) and PLA2 regions in the VP1u were obtained from ImmunoGlobe (Himmelstadt, Germany). The polyclonal goat IgG against human serpinA3 and the polyclonal sheep IgG against ITIH4 were purchased from R&D systems (Minneapolis, MN). SerpinA3 and ITIH4 were detected by Western blot using a secondary rabbit anti-goat and anti-sheep IgG (H + L) HRP, respectively (Thermo Fisher Scientific). The monoclonal mouse antibody 3113-81 C (US Biological, Boston, MA) was used for the detection of the viral protein VP2 by Western blot. Active kallikrein from human plasma and α-chymotrypsin from bovine pancreas were purchased from Sigma-Aldrich. Recombinant ITIH4 was kindly provided by S.Thiel (University of Aarhus, Denmark).

Infectivity assay

Virus infectivity was examined by quantification of NS1 mRNA. Equal amounts of progeny and plasma B19V were incubated with UT7/Epo cells. After 30 min (input), 24 h and 48 h, cells were transferred to RNase-free tubes (Safe-Lock Tubes 1.5 mL, Eppendorf Biopur®) and pelleted. The pellet was washed twice with PBS and total RNA was extracted with GenCatch Total RNA Miniprep Kit (Epoch Life Sciences, Missouri City, TX) according to the manufacturer's protocol. The extracted samples were treated with DNase I for 30 min at 37 °C, and NS1 mRNA was quantified as described elsewhere[60].

Immunoprecipitation

For immunoprecipitation of plasma-derived or progeny viruses, antibodies against the capsid (860-55D, Caps), serpinA3 and ITIH4 were incubated with the virus for 1 h at 4 °C. After overnight incubation with 20 µl protein G agarose beads in LoBind tubes (Eppendorf, Hamburg, Germany) at 4 °C, the beads were washed four times (three times with PBSA-1% bovine serum albumin and once with PBS) and resuspended in protein loading buffer to analyze the immunoprecipitated capsids by Western blotting or in PBS to quantify the viral DNA by qPCR. Total DNA was extracted using the DNeasy blood and tissue kit (Qiagen, Hilden, Germany) and quantified as specified above.

Generation of B19V progeny and binding to protease inhibitors

Progeny virions were generated in cell culture by using erythroid progenitor cells (EPCs) and hypoxia conditions. Primary CD36+ EPCs (3×10^5) cultured under hypoxia (1% O_2) for 2 days, were infected with B19V at 10^4 geq per cell for 1 h at 37 °C. The cells were washed to remove unbound viruses and further incubated at 37 °C. At different post-infection times, the supernatant was collected and used for B19V DNA quantification, immunoprecipitation, iodixanol density gradient ultracentrifugation, and infectivity assay. Progeny virions were incubated with plasma devoid of B19V and B19V-specific antibodies, diluted 1:100 for 1 h at 37 °C. For ITIH4 binding, plasma was supplemented with 1 mM $MgCl_2$ and 10 μM $NiSO_4$ to allow binding through the metal-ion dependent adhesion site (MIDAS) within the von Willebrand factor A domain[37]. Virions were immunoprecipitated with antibodies against capsid (860-55D), serpinA3, ITIH4 and quantified by qPCR.

Protease inhibition activity in vitro

A chymotrypsin activity fluorometric assay was performed to detect protease inhibition activity in virions purified and concentrated from patient samples. B19V VLPs were used as a negative control. To measure peptidase activity, quenched fluorogenic peptide substrates were used (R&D systems, ES002). Recombinant human serpinA3 (R&D systems, 1295-PI) or purified B19V were incubated with α-chymotrypsin from bovine pancreas (Sigma-Aldrich, C3142) using a molar serpin to protease ratio of 20:1. The reaction was performed at 37 °C for 30 min in 50 mM Tris, 10 mM $CaCl_2$, 150 mM NaCl, 0.05% (w/v) Brij-35 (TCNB), at pH 7.5. A fluorogenic substrate MCA-Arg-Pro-Lys-Pro-Val-Glu-NVAL-Trp-Arg-Lys(DNP)-NH_2 (20 µM; R&D systems, ES002) was added to the serpin-protease mixture in F16 Black Maxisorp Plate (Nunc, 475515) and the fluorescence was read in kinetic mode for 5 min at excitation and emission wavelengths of 320 nm and 405 nm, respectively.

Detection of serpinA3-protease suicide complexes

Recombinant human serpinA3 or purified B19V were incubated with α-chymotrypsin from bovine pancreas as described above. Proteins were resolved on a 10% SDS-PAGE and transferred to a PVDF membrane. The

membrane was blocked overnight at 4 °C with 5% milk in TBS-T. SerpinA3 was detected using the same antibody described above followed by chemiluminescent detection using a HRP-coupled rabbit anti-goat IgG (H + L).

Proteolytic cleavage of ITIH4

Recombinant human ITIH4 or purified B19V were incubated with active plasma kallikrein (Sigma-Aldrich, 2638), using a molar ITIH4 to protease ratio of 3:1. The reaction was performed at 37 °C for 6 and 8 h in TBS, 2 mM $CaCl_2$ and 2 mM MgCl2. Proteins were resolved on a 10% SDS-PAGE and transferred to a PVDF membrane as described above. Intact and cleaved ITIH4 were detected using a polyclonal sheep antibody (R&D systems, AF-8157) followed by chemiluminescent detection using an HRP-coupled donkey anti-sheep IgG (H + L).

Analysis of host protein dissociation from virus

UT7/Epo cells (3×10^5) were infected with plasma-derived B19V particles (3×10^{10}) for 1 h at 4 °C to allow virus attachment and washed three times with ice-cold PBS to remove unbound virus. For virus internalization, the cells were pre-incubated with 50 nM BafA1 or 0.1% DMSO (control) for 30 min prior to infection for 30 min at 37 °C. The cells were washed three times with ice-cold PBS and trypsinized for 4 min at 37 °C to remove non-internalized viruses. Cells were lysed in NP-40 lysis buffer (50 mM Tris-HCl, 150 mM NaCl, 1% NP-40, 5 mM EDTA) supplemented with protease inhibitor cocktail (Complete Mini; Roche, Basel, Switzerland). As a control, mock-infected cells were lysed and spiked with the virus. B19V capsids were immunoprecipitated with antibodies against intact capsid, serpinA3 or ITIH4 as described above, and immunoprecipitated virions were quantified by qPCR.

Statistical analysis

Data analysis was performed using GraphPad Prism. Data points are presented as mean values, and error bars represent SDs. Statistical tests are detailed in the respective figure legends.

Negative staining and cryoEM sample preparation

Purified B19V virus preparations were applied to glow-discharged carbon coated 300 mesh grids at a volume of 3 μL with 2% phosphotungstic acid (PTA). Negatively stained B19V unheated control and heated treatments were screened on the Tecnai BioTwin Spirit to verify concentration and integrity for single particle analysis (SPA) data collection. Vitrification (Vitrobot; Thermo Fisher Scientific) after negative staining was done with continuous carbon QUANTIFOIL (QFs) R2/1 grid (QUANTIFOIL, Germany) which were glow discharged using the PELCO easiGlow Glow Discharge System for TEM Grids (Ted Pella, Redding CA). Sample volumes of 3.0 μL were applied to continuous carbon R2/1 QFs with a wait time of 60 s immediately preceding liquid ethane submersion. Grids are stored in liquid nitrogen until preliminary screening on the Penn State Titan Krios (Thermo Fisher Scientific) to determine optimal grids for data collection and acquisition.

CryoEM data acquisition

Vitrified B19V virions were collected on the Titan Krios using EPU Software at 59,000X magnification and 300 kV with a spherical aberration correction. The calibrated pixel size was 1.08 Å/pixel. Image stacks of 49 frames were collected with a total electron dose of 2.5 $e^-/Å^2$/frame (100 e-/Å2) using a Falcon III Direct Electron Detector (Supplementary Table 1). This was done to enhance the contrast of the protein-coated virions on continuous carbon 2/1 Quantifoils. Total micrographs, particles, and subparticles are reported for each dataset (Supplementary Table 1).

CryoEM image processing

The image processing for the icosahedral reconstruction was performed in CryoSPARC[61], including patch motion Correction, patch CTF estimation, particle picking, 2D/3D classification, ab initio model generation, and homogeneous refinement. Particles were initially picked by 'blob picker' and then automatically selected using 'template picker.' Iterative rounds of 2D and 3D Classification were performed in CryoSPARC to remove bad classes from further processing, and an initial model was generated from the final particle subset. Homogenous refinement was performed in CryoSPARC with additional global/local CTF refinements.

Subparticle reconstruction for serpinA3 and ITIH4

Subparticles were designated and extracted using ISECC (Icosahedral Extraction and Correlative Classification)[62]. Subvolumes were then 3D classified without symmetry or alignments in RELION[63]. Relevant classes were pooled, and subparticle density was recombined into the icosahedral maps using symbreak within ISECC[62]. The resulting asymmetric maps were postprocessed in DeepEMhancer[64] and RELION[63]. For local refinement of the subvolume, subparticles for the relevant classes were imported into cryoSPARC and Local Refinement was performed with various masks targeted for each protease inhibitor density or a larger area including a capsid region, with pose/shift gaussian prior applied during alignment[61].

Model building and refinement

A model for the B19V-VLP (PDB ID 1S58) was used to initiate the build of the B19V. In parallel, ModelAngelo was employed with the B19V sequence (UniProt access code: Q76T42) as an input reference for de novo modeling[26]. Regions and residues exhibiting disparities between the two models were meticulously scrutinized in conjunction with the cryoEM density and subsequently rectified. The model for an uncleaved S-conformation serpinA3 variant (PDB ID 6HGE) was mutated to the wild-type sequence (NP_001371603.1) and used to initiate the build of B19V-bound serpinA3. First, the initial model was refined against the refined subvolume of serpinA3 (Supplementary Table 1). Then the refined serpinA3 model and the atomic coordinates corresponding to six VP2s around the twofold symmetry axis were refined simultaneously against the B19V-serpinA3 asymmetric map. The refinements were performed first in ISOLDE[65] and subsequently in PHENIX[66] before validation with MolProbity[67] (Supplementary Table 1). This second round of refinement in the full complex asymmetric map aimed to minimize the clashes between molecules and adjust for any conformational variations from the icosahedral structure. A homology model for ITIH4 was generated using SWISS-MODEL (https://swissmodel.expasy.org/)[38], while Alphafold was employed to predict the complete sequence of ITIH4 (UniProt access code: Q14624) (AlphaFold entry: Q14624)[39].

Structure analysis and display

Local resolutions were estimated by using local_resolution function in Phenix[68]. Contacts between B19V and host molecules were identified as residues having atoms separated by less than 0.4-Å van der Waal's radius in ChimeraX[69]. The roadmap for footprints of the host proteins and neutralizing antibodies was generated in RIVEM[41]. Map visualization and images were generated in ChimeraX[69].

Reporting summary

Further information on research design is available in the Nature Portfolio Reporting Summary linked to this article.

Data availability

The cryoEM maps and atomic coordinates of the B19V capsids and host proteins have been deposited in the EM database (https://www.emdatabank.org) and protein data bank (https://www.rcsb.org) under accession codes EMD-45136 (PDB entry 9C27), EMD-45160 (PDB entry 9C2T), EMD-46607 (PDB entry 9D7K), EMD- 45184 (PDB entry 9C4F), and EMD-45191 (PDB entry 9C4N) for B19V, B19V-serpinA3 complex,

serpinA3-alone, B19V-ITIH4 complex, and ITIH4-fragment, respectively. Source data are provided with this paper.

References

1. Brown, K. E. et al. Parvovirus B19 in human disease. *Annu. Rev. Med.* **48**, 59–67 (1997).
2. Heegaard, E. D. & Brown, K. E. Human Parvovirus B19. *Clin. Microbiol. Rev.* **15**, 485–505 (2002).
3. Smith-Whitley, K. et al. Epidemiology of human parvovirus B19 in children with sickle cell disease. *Blood* **103**, 422–427 (2004).
4. Parilla, B., Tamura, R. & Ginsberg, N. Association of Parvovirus infection with isolated fetal effusions. *Am. J. Perinatol.* **14**, 357–358 (1997).
5. Koch, W. C., Harger, J. H., Barnstein, B. & Adler, S. P. Serologic and virologic evidence for frequent intrauterine transmission of human parvovirus B19 with a primary maternal infection during pregnancy. *Pediatr. Infect. Dis. J.* **17**, 489–494 (1998).
6. Marano, G. & Vaglio, S. Human Parvovirus B19 and blood product safety: a tale of twenty years of improvements. *Blood Transfus.* https://doi.org/10.2450/2014.0174.14 (2014).
7. Ozawa, K., Kurtzman, G. & Young, N. Replication of the B19 Parvovirus in human bone marrow cell cultures. *Science* **233**, 883–886 (1986).
8. Takahashi, T., Ozawa, K., Takahashi, K., Asano, S. & Takaku, F. Susceptibility of human erythropoietic cells to B19 parvovirus in vitro increases with differentiation. *Blood* **75**, 603–610 (1990).
9. Wolfisberg, R., Ruprecht, N., Kempf, C. & Ros, C. Impaired genome encapsidation restricts the in vitro propagation of human parvovirus B19. *J. Virol. Methods* **193**, 215–225 (2013).
10. Ozawa, K. & Young, N. Characterization of capsid and noncapsid proteins of B19 parvovirus propagated in human erythroid bone marrow cell cultures. *J. Virol.* **61**, 2627–2630 (1987).
11. Kaufmann, B., Simpson, A. A. & Rossmann, M. G. The structure of human parvovirus B19. *Proc. Natl Acad. Sci. USA* **101**, 11628–11633 (2004).
12. Leisi, R., Di Tommaso, C., Kempf, C. & Ros, C. The receptor-binding domain in the VP1u region of Parvovirus B19. *Viruses* **8**, 61 (2016).
13. Ros, C., Gerber, M. & Kempf, C. Conformational changes in the VP1-Unique region of native human Parvovirus B19 lead to exposure of internal sequences that play a role in virus neutralization and infectivity. *J. Virol.* **80**, 12017–12024 (2006).
14. Rosenfeld, S. J., Young, N. S., Alling, D., Ayub, J. & Saxinger, C. Subunit interaction in B19 parvovirus empty capsids. *Arch. Virol.* **136**, 9–18 (1994).
15. Sato, H. et al. Identification and mapping of neutralizing epitopes of human parvovirus B19 by using human antibodies. *J. Virol.* **65**, 5485–5490 (1991).
16. Yoshimoto, K. et al. A second neutralizing epitope of B19 parvovirus implicates the spike region in the immune response. *J. Virol.* **65**, 7056–7060 (1991).
17. Brown, C. S. et al. Localization of an immunodominant domain on baculovirus-produced parvovirus B19 capsids: correlation to a major surface region on the native virus particle. *J. Virol.* **66**, 6989–6996 (1992).
18. Sun, Y., Klose, T., Liu, Y., Modrow, S. & Rossmann, M. G. Structure of Parvovirus B19 decorated by fabs from a human antibody. *J. Virol.* **93**, e01732–18 (2019).
19. Saikawa, T., Anderson, S., Momoeda, M., Kajigaya, S. & Young, N. S. Neutralizing linear epitopes of B19 parvovirus cluster in the VP1 unique and VP1-VP2 junction regions. *J. Virol.* **67**, 3004–3009 (1993).
20. Kajigaya, S. et al. Self-assembled B19 parvovirus capsids, produced in a baculovirus system, are antigenically and immunogenically similar to native virions. *Proc. Natl Acad. Sci. USA* **88**, 4646–4650 (1991).
21. Agbandje, M., Kajigaya, S., McKenna, R., Young, N. S. & Rossmann, M. G. The structure of human Parvovirus B19 at 8 Å; resolution. *Virology* **203**, 106–115 (1994).
22. Kaufmann, B., Chipman, P. R., Kostyuchenko, V. A., Modrow, S. & Rossmann, M. G. Visualization of the externalized VP2 N termini of infectious human Parvovirus B19. *J. Virol.* **82**, 7306–7312 (2008).
23. Cotmore, S. F., Hafenstein, S. & Tattersall, P. Depletion of virion-associated divalent cations induces Parvovirus minute virus of mice to eject its genome in a 3′-to-5′ direction from an otherwise intact viral particle. *J. Virol.* **84**, 1945–1956 (2010).
24. Bönsch, C., Kempf, C. & Ros, C. Interaction of Parvovirus B19 with human erythrocytes alters virus structure and cell membrane integrity. *J. Virol.* **82**, 11784–11791 (2008).
25. Henderson, R. & Hasnain, S. 'Cryo-EM': electron cryomicroscopy, cryo electron microscopy or something else? *IUCrJ* **10**, 519–520 (2023).
26. Jamali, K. et al. Automated model building and protein identification in cryo-EM maps. *Nature* **628**, 450–457 (2024).
27. Pintilie, G. et al. Measurement of atom resolvability in cryo-EM maps with Q-scores. *Nat. Methods* **17**, 328–334 (2020).
28. Goetschius, D. J., Lee, H. & Hafenstein, S. CryoEM reconstruction approaches to resolve asymmetric features. in *Adv. Virus Res.* **105**, 73–91 (2019).
29. Bost, F., Diarra-Mehrpour, M. & Martin, J.-P. Inter-alpha-trypsin inhibitor proteoglycan family. A group of proteins binding and stabilizing the extracellular matrix. *Eur. J. Biochem.* **252**, 339–346 (1998).
30. Briggs, D. C. et al. Inter-α-inhibitor heavy chain-1 has an integrin-like 3D structure mediating immune regulatory activities and matrix stabilization during ovulation. *J. Biol. Chem.* **295**, 5278–5291 (2020).
31. Gardill, B. R., Schmidt, K. & Muller, Y. A. NewBG: a surrogate corticosteroid-binding globulin with an unprecedentedly high ligand release efficacy. *J. Struct. Biol.* **207**, 169–182 (2019).
32. Gigler, A. et al. Generation of neutralizing human monoclonal antibodies against Parvovirus B19 proteins. *J. Virol.* **73**, 1974–1979 (1999).
33. Zolotukhin, S. et al. Recombinant adeno-associated virus purification using novel methods improves infectious titer and yield. *Gene Ther.* **6**, 973–985 (1999).
34. Wolfisberg, R., Kempf, C. & Ros, C. Late maturation steps preceding selective nuclear export and egress of progeny Parvovirus. *J. Virol.* **90**, 5462–5474 (2016).
35. Gettins, P. G. W. Serpin structure, mechanism, and function. *Chem. Rev.* **102**, 4751–4804 (2002).
36. Maas, C. & De Maat, S. Therapeutic SERPINs: improving on nature. *Front. Cardiovasc. Med.* **8**, 648349 (2021).
37. Pihl, R. et al. ITIH4 acts as a protease inhibitor by a novel inhibitory mechanism. *Sci. Adv.* **7**, eaba7381 (2021).
38. Waterhouse, A. et al. SWISS-MODEL: homology modelling of protein structures and complexes. *Nucleic Acids Res.* **46**, W296–W303 (2018).
39. Jumper, J. et al. Highly accurate protein structure prediction with AlphaFold. *Nature* **596**, 583–589 (2021).
40. Lee, H. et al. Transferrin receptor binds virus capsid with dynamic motion. *Proc. Natl Acad. Sci. USA* **116**, 20462–20471 (2019).
41. Xiao, C. & Rossmann, M. G. Interpretation of electron density with stereographic roadmap projections. *J. Struct. Biol.* **158**, 182–187 (2007).
42. Chen, A. Y., Kleiboeker, S. & Qiu, J. Productive Parvovirus B19 infection of primary human erythroid progenitor cells at Hypoxia is regulated by STAT5A and MEK signaling but not HIFα. *PLoS Pathog.* **7**, e1002088 (2011).

43. Norja, P. et al. Bioportfolio: lifelong persistence of variant and prototypic erythrovirus DNA genomes in human tissue. *Proc. Natl Acad. Sci. USA* **103**, 7450–7453 (2006).
44. Corcioli, F. et al. Tissue persistence of parvovirus B19 genotypes in asymptomatic persons. *J. Med. Virol.* **80**, 2005–2011 (2008).
45. Caliaro, O. et al. Parvovirus B19 uncoating occurs in the cytoplasm without capsid disassembly and it is facilitated by depletion of capsid-associated divalent cations. *Viruses* **11**, 430 (2019).
46. Kwong, P. D. et al. HIV-1 evades antibody-mediated neutralization through conformational masking of receptor-binding sites. *Nature* **420**, 678–682 (2002).
47. Lin, J., Cheng, N., Hogle, J. M., Steven, A. C. & Belnap, D. M. Conformational shift of a major Poliovirus antigen confirmed by immuno-cryogenic electron microscopy. *J. Immunol.* **191**, 884–891 (2013).
48. Lindesmith, L. C. et al. Conformational occlusion of blockade antibody epitopes, a novel mechanism of GII.4 human norovirus immune evasion. *mSphere* **3**, e00518–17 (2018).
49. Tate, M. et al. Playing hide and seek: how glycosylation of the influenza virus hemagglutinin can modulate the immune response to infection. *Viruses* **6**, 1294–1316 (2014).
50. Mascola, J. R. & Montefiori, D. C. HIV-1: nature's master of disguise. *Nat. Med.* **9**, 393–394 (2003).
51. Feng, Z., Hirai-Yuki, A., McKnight, K. L. & Lemon, S. M. Naked viruses that aren't always naked: quasi-enveloped agents of acute hepatitis. *Annu. Rev. Virol.* **1**, 539–560 (2014).
52. Lindblom, A. et al. Slow clearance of human Parvovirus B19 viremia following acute infection. *Clin. Infect. Dis.* **41**, 1201–1203 (2005).
53. Lefrere, J.-J. Persistent B19 infection in immunocompetent individuals: implications for transfusion safety. *Blood* **106**, 2890–2895 (2005).
54. Candotti, D., Etiz, N., Parsyan, A. & Allain, J.-P. Identification and characterization of persistent human erythrovirus infection in blood donor samples. *J. Virol.* **78**, 12169–12178 (2004).
55. Upton, C., Macen, J. L., Wishart, D. S. & McFadden, G. Myxoma virus and malignant rabbit fibroma virus encode a serpin-like protein important for virus virulence. *Virology* **179**, 618–631 (1990).
56. Lomas, D. A., Evans, D. L., Upton, C., McFadden, G. & Carrell, R. W. Inhibition of plasmin, urokinase, tissue plasminogen activator, and C1S by a myxoma virus serine proteinase inhibitor. *J. Biol. Chem.* **268**, 516–521 (1993).
57. Bao, J. et al. Serpin functions in host-pathogen interactions. *PeerJ* **6**, e4557 (2018).
58. Irmscher, S. et al. Kallikrein Cleaves C3 and Activates Complement. *J. Innate Immun.* **10**, 94–105 (2018).
59. Baker, C. SERPINA3 (aka alpha-1-antichymotrypsin). *Front. Biosci.* **12**, 2821 (2007).
60. Suter, C. et al. Globoside and the mucosal pH mediate parvovirus B19 entry through the epithelial barrier. *PLoS Pathog.* **19**, e1011402 (2023).
61. Punjani, A., Rubinstein, J. L., Fleet, D. J. & Brubaker, M. A. cryoSPARC: algorithms for rapid unsupervised cryo-EM structure determination. *Nat. Methods* https://doi.org/10.1038/nmeth.4169 (2017).
62. Goetschius, D. J. et al. High resolution cryo EM analysis of HPV16 identifies minor structural protein L2 and describes capsid flexibility. *Sci. Rep.* **11**, 3498 (2021).
63. Kimanius, D., Dong, L., Sharov, G., Nakane, T. & Scheres, S. H. W. New tools for automated cryo-EM single-particle analysis in RELION-4.0. *Biochem. J.* **478**, 4169–4185 (2021).
64. Sanchez-Garcia, R. et al. DeepEMhancer: a deep learning solution for cryo-EM volume post-processing. *Commun. Biol.* **4**, 874 (2021).
65. Croll, T. I. *ISOLDE*: a physically realistic environment for model building into low-resolution electron-density maps. *Acta Crystallogr. D. Struct. Biol.* **74**, 519–530 (2018).
66. Afonine, P. V. et al. Real-space refinement in *PHENIX* for cryo-EM and crystallography. *Acta Crystallogr. D. Struct. Biol.* **74**, 531–544 (2018).
67. Chen, V. B. et al. *MolProbity*: all-atom structure validation for macromolecular crystallography. *Acta Crystallogr. Sect. D. Biol. Crystallogr.* **66**, 12–21 (2010).
68. Adams, P. D. et al. *PHENIX*: a comprehensive Python-based system for macromolecular structure solution. *Acta Crystallogr. Sect. D. Biol. Crystallogr.* **66**, 213–221 (2010).
69. Goddard, T. D. et al. UCSF ChimeraX: meeting modern challenges in visualization and analysis: UCSF ChimeraX visualization system. *Protein Sci.* **27**, 14–25 (2018).

Acknowledgements

This study was supported by a grant from the Swiss National Science Foundation (SNSF grant 320030_207850 to C.R.). We are grateful to J. Blümel (Paul-Ehrlich Institute, Germany) for providing the plasma donation infected with genotype 2, and to S.Thiel (University of Aarhus, Denmark) for providing the recombinant ITIH4. The co-authors would like to acknowledge the Huck Institutes' Cryo Electron Microscopy (Facility (RRID:SCR_024456) for use of the Thermo Fisher Titan Krios.

Author contributions

H.L. performed the cryoEM structural analysis, and drafted the original manuscript. R.A. performed the experiments, data collection and analysis, contributed to the review and editing of the manuscript. H.L. and R.A. contributed equally to this study and shared the co-first authorship. S.L.H. contributed to the study concept and design, secured funding, and drafted the original manuscript. C.R. contributed to the study concept and design, performed data analysis, secured funding, and drafted the original manuscript. S.L.H. and C.R. contributed equally to this study and shared the co-corresponding authorship. N.M.D. and C.M.B. performed cryoEM sample vitrification and data collection. S.S., D.G., and N.M.D. contributed to the cryoEM data analysis. J.B. and R.L. optimized virus purification for cryo-EM, contributed to the mass spectrometry analysis.

Competing interests

The authors declare no competing interests.

Ethical approval

The University of Minnesota Hormel Institute and University of Bern are committed to maintaining a safe and respectful environment for all researchers, students, and staff members to the advancement of all and benefit of everyone.

Additional information

Supplementary information The online version contains supplementary material available at https://doi.org/10.1038/s41467-024-53794-1.

Correspondence and requests for materials should be addressed to Susan L. Hafenstein or Carlos Ros.

Peer review information *Nature Communications* thanks Vidya Mangala Prasad and the other anonymous reviewer(s) for their contribution to the peer review of this work. A peer review file is available